SCIENTIFIC REPORTS

OPEN

Received: 6 October 2017
Accepted: 5 June 2018
Published online: 07 August 2018

In situ viscoelastic properties and chain conformations of heavily hydrated carboxymethyl dextran layers: a comparative study using OWLS and QCM-I chips coated with waveguide material

Andras Saftics[1,2], György Aurél Prósz[1], Barbara Türk[1,2], Beatrix Peter[1], Sándor Kurunczi[1] & Robert Horvath[1]

Hydration, viscoelastic properties and dominant structure of thin polymer layers on the surface of waveguide material were evaluated using optical waveguide lightmode spectroscopy (OWLS) and quartz crystal microbalance (QCM) methods. The fundamentally different principles of the two applied label-free biosensors enable to examine analyte layers from complementary aspects, e.g. to determine the amount of bound water in hydrated layers. In this study, a new QCM instrument with impedance measurement (QCM-I) is introduced. Its specially designed sensor chips, covered by thin film of waveguide material, supply identical surface as used in OWLS sensors, thus enabling to perform parallel measurements on the same type of surface. Viscoelastic analysis of the measured data was performed by our evaluation code developed in MATLAB environment, using the Voinova's Voigt-based model. *In situ* deposition experiments on the ultrathin films of poly(L-lysine)-*graft*-poly(ethylene glycol) (PLL-*g*-PEG) were conducted for instrumental and code validation. Additionally, a novel OWLS-QCM data evaluation methodology has been developed based on the concept of combining hydration and viscoelastic data with optical anisotropy results from OWLS measurements. This methodology provided insight into the time-dependent chain conformation of heavily hydrated nano-scaled layers, resulting in unprecedented structural, hydration and viscoelastic information on covalently grafted ultrathin carboxymethyl dextran (CMD) films. The measured mass values as well as hydration and viscoelastic properties were compared with the characteristics of PLL-*g*-PEG layers.

Label-free biosensing offers a number of opportunities for exploring phenomena which have been hidden from the field of view of conventional labeling techniques. The main attractive consequence of the label-free principle is the elimination of disturbing effect and cost of label molecules as well as the ability to measure the kinetic behavior of interactions even at the sub-molecular level by allowing real-time monitoring (while the conventional labeling methods provide only end-point data of biomolecular and cellular interactions)[1]. Several label-free transduction principles have been reported and proven to be suitable for pharmaceutical industry or healthcare, i.e. for point-of-care testing, and their applications in basic researches are on the rise[2,3]. Regarding the applied transduction method, label-free biosensors can be generally classified as electrical, optical and mechanical techniques which can usually provide complementary results.

Label-free optical biosensors are principally based on the measurement of refractive index change originated from the presence of analytes on the optical transducer surface. The sensitive waveguide based techniques have

[1]Nanobiosensorics Laboratory, Centre for Energy Research, Hungarian Academy of Sciences, Konkoly Thege Miklós út 29-33, Budapest, 1121, Hungary. [2]Faculty of Chemical Technology and Biotechnology, Budapest University of Technology and Economics, Műegyetem rkp. 3, Budapest, 1111, Hungary. Correspondence and requests for materials should be addressed to R.H. (email: horvathr@mfa.kfki.hu)

presented their performances in several applications, including *in situ* monitoring of the construction of polyelectrolyte multilayers[4–6], adsorption of biomolecules[7] as well as monitoring the adhesion of living cells[8]. Beside the simplest and most traditional optical waveguide lightmode spectroscopy (OWLS) technique, the recently introduced waveguide-based instruments, such as resonant waveguide grating (RWG) and grating coupled interferometry (GCI) biosensors have shown the potentials of this measurement principle in terms of throughput and achieving top sensitivities[3,9,10]. Apart from the plentiful applications, an important limitation of these techniques is that the water, "trapped" in the analyte layers, cannot be detected, because all of these devices are monitoring refractive index contrast compared to the aqueous background. This fact means that only the "dry" mass of analyte molecules or living cells can be determined[11,12].

Quartz crystal microbalance (QCM) is a mechanical label-free biosensor that measures the shift in resonance frequency of the quartz crystal generated by the deposited analyte molecules or cells on its surface. This technique is able to measure the hydrated mass of the examined layers, since the frequency shift is sensitive to the surface-bound water as well. Furthermore, viscoelastic properties of layers can be gained by the *in situ* monitoring of energy dissipation that is usually related to the presence of soft, hydrated films on the sensor surface. QCM has shown its potentials, especially for investigating highly hydrated layers formed by both synthetic polymers or biomaterials[13–16].

Due to the complexity and nano-scale dimensions of the studied objects on surfaces, complementary analytical techniques afford better insight into the structure and behavior of layers, especially in case of heavily hydrated ultrathin films. The combination of QCM data with results obtained from optical methods is an attractive tool for characterizing the hydration properties of the formed thin films of biopolymers, because measuring the dry and hydrated mass provides quantitative information about the amount of bound water inside the analyte layer[17]. Precedent combined techniques are the simultaneous QCM-SPR[18,19] and QCM-ellipsometry[20] measurements, however, only few cases have been presented when the technique can be applied on the same surface enabling simultaneous measurements exactly on the same target objects (ellipsometry compatible QCM module)[21,22]. In spite of the expanding field of combined label-free instruments and the advantages of waveguide based methods over SPR and ellipsometry, so far the realization of an instrumental combination of the OWLS or other waveguide-based methods with a mechanical principle based technique such as QCM is still missing. The combinations of QCM and OWLS data obtained from parallel measurements can be however prosperously applied[11,12,23].

In the present study, a new compact QCM instrument the so-called QCM-I (QCM with impedance measurement), developed and launched by MicroVacuum Ltd. (Budapest, Hungary), was used to interrogate QCM chips. Compared to the conventional setups, QCM-I applies a different method for obtaining simultaneous frequency and dissipation data. Dissipation can be measured by two types of read-out techniques in QCM devices[24]: (*i*) using impulse excitation method (also called as ring-down method) with the measurement of the decay of crystal's oscillation after the excitation has been turned off, or (*ii*) by impedance analysis using a network analyzer that measures the frequency spectrum of impedance. The widely used QCM instruments with the trademark of QCM-D (QCM with dissipation monitoring), commercialized by QSense (Biolin Scientific, Sweden) apply the ring-down method[25].

Numerous ultrathin interface layers have been already introduced for practical applications, however, many of their structure and properties are shallowly explored due to the lack of techniques which would be able to allow broad insight, especially when the measurement is conducted in the presence of solvent, e.g. in aqueous environments. Ultrathin films constructed of highly hydrated polymers such as dextran or poly(L-lysine)-*graft*-poly(ethylene glycol) (PLL-*g*-PEG) are good examples for layers which firmly represents the difficulties in their analysis. The glucose based biopolymer dextran[26–29] and the synthetic polymer PLL-*g*-PEG[30,31] are used as coating materials in label-free biosensors, primarily for reducing the non-specific binding, the dominating issue of protein adsorption when measurements are conducted in complex matrices. The advanced hydrophilicity of these polymer chains is supposed to have a principal role in the protein resistant ability[32,33]. Due to the hydrophilic characteristic, the formation of dextran and PLL-*g*-PEG layers accompanies with a high water enrichment in the layer, as a large amount of water can be bound and trapped by the polymer chains[27]. Whilst PLL-*g*-PEG layers are stabilized by electrostatic interactions between the negatively charged oxide surfaces and positively charged PLL backbone[30], dextran coatings are generally fabricated using privileging methods for covalent grafting[26,34,35]. Instead of native dextran, many applications prefer carboxymethyl dextran (CMD) due to the ease of conjugation with receptor molecules and chemical possibility to attach the polymer chains covalently to transducer surfaces. One possible way to graft CMD to silicon-oxide type surfaces is the reaction of amino groups of the aminosilylated surface with CMD, activated by carbodiimide and succinimide reagents on its carboxyl moieties in order to generate amide bonds[36,37]. This "grafting to" method yields relatively low-density CMD chains on the surface with mostly trains and few loops among the possible chain conformations. In our previous study[37], we first explored the optical anisotropy of such covalently grafted CMD chains, by measurements using the *in situ* OWLS technique. As we presented in that paper, an overestimated refractive index of the CMD layer was measured owing to the prevalently lain down chain conformation which accompanied with an underestimated value in the calculated layer thickness as well. We proposed QCM-I to be a promising method to clarify the realistic thickness of the CMD layer, to determine its hydration degree and viscoelastic properties, as well as to analyze the anisotropic characteristic and chain conformation in terms of hydration behavior. As the best of our knowledge, OWLS and QCM data have never been combined for time-dependent optogeometric analysis as a function of hydration or viscoelasticity, potentially revealing chain conformations and reorientations. Despite the CMD is a common material in biosensor applications, viscoelastic analysis of covalently grafted ultrathin CMD films is also missing from the available publications and the hydration properties and the time-dependent structure of these layers are still not deeply understood.

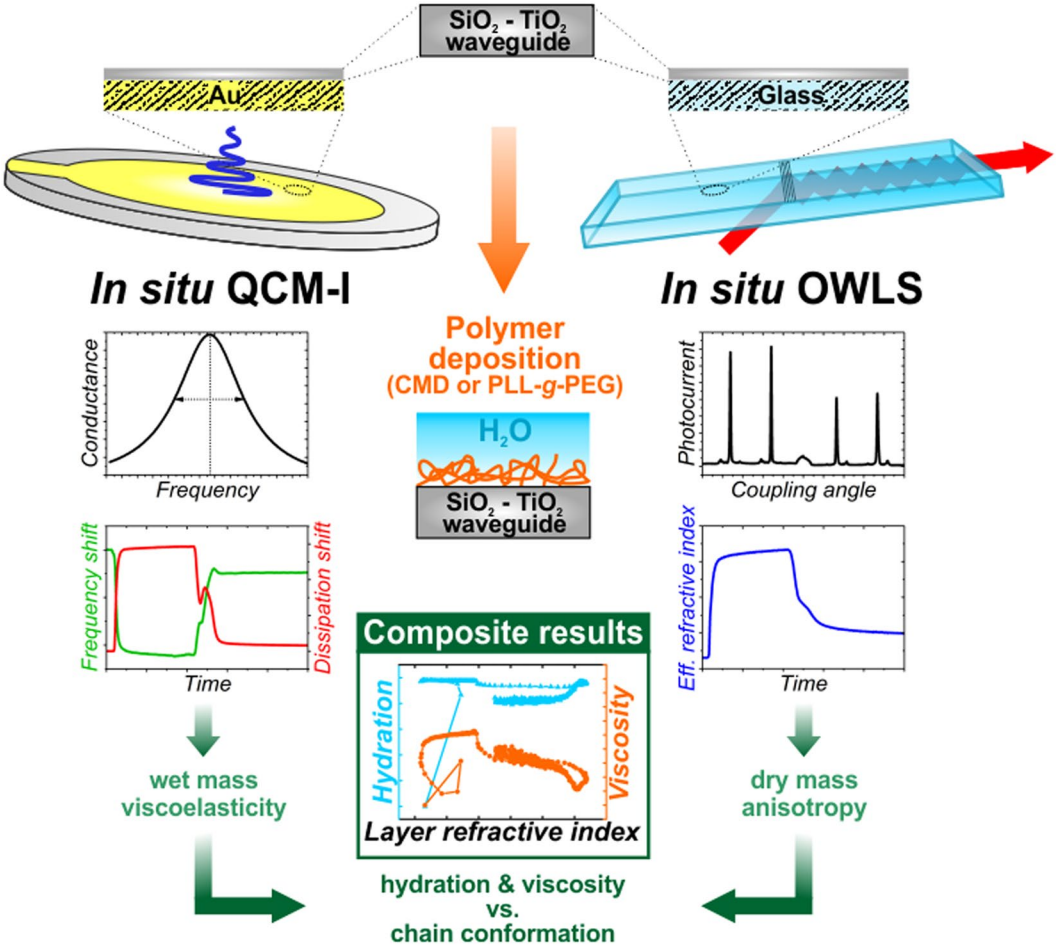

Figure 1. Schematic representation of the measurement and data evaluation methodology developed and applied in this work.

In the present work, we introduce a recently developed QCM-I instrument fitted to parallel OWLS measurements by employing specially designed QCM-I chips with a film of SiO_2-TiO_2 waveguide material on top of the gold layer. These developments are able to open the way to parallel OWLS and QCM measurements on exactly the same type of surfaces. In order to demonstrate its capabilities, the formation of CMD and PLL-*g*-PEG layers on the surface was measured *in situ* and the obtained kinetic QCM-I data were analyzed by our MATLAB code. The mass values obtained from the *in situ* QCM-I experiments were supported by *in situ* OWLS data from parallel experiments. The applied methodology allowed to determine and compare the hydration degree of the ultrathin, physically adsorbed PLL-*g*-PEG and covalently grafted CMD layers. In addition to this conventional data analysis method, we present a novel protocol that we developed in order to simultaneously characterize chain conformation and hydration at different layer formation phases and provide a general tool for achieving new insight into the behavior of heavily hydrated ultrathin layers. Using this method, we could make further deductions for the developed CMD layers in terms of dominating conformation of hydrated chains (the applied methodology is schematically represented in Fig. 1). Whilst such examinations are rare and insufficient in the literature for CMD layers, more data are available for the PLL-*g*-PEG (e.g.: deposited mass, viscoelastic and hydration properties). Our measurements on PLL-*g*-PEG layers were able to provide adequate basis for validating the data obtained from measurements with the QCM-I device and verifying our results on CMD films which have not been reported so far.

Results

Viscoelastic properties of CMD and PLL-*g*-PEG layers. There are some simple data representation methods which are useful to demonstrate how adequately the Sauerbrey equation can be applied for calculating the mass of a specific layer. At the first glance, the comparison of $\Delta f_n/n$, the values of the normalized frequency shift at given n overtones can be rather suggestive[38], because a significant dependence of $\Delta f_n/n$ on the overtone number implies a viscoelastic case. Additionally, the magnitude of dissipation shift at the examined n overtones (ΔD_n) can be also a good indicator. Critical number of 2×10^{-6} for dissipation shift has been proposed as the upper limit for treating a layer as rigid[39,40].

Table 1 summarizes the $\Delta f_n/n$ and ΔD_n values for the irreversibly attached layers. Due to the sensitivity of fundamental frequency ($n = 1$) to the environmental noise[38], fundamental resonance parameters were usually

		PLL-*g*-PEG	CMD
$\Delta f_n/n$ (Hz)	$n=3$	-32.5 ± 3.7	-15.7 ± 1.6
	$n=5$	-30.6 ± 4.3	-14.7 ± 1.6
	$n=7$	-29.2 ± 4.8	-14.3 ± 1.9
$\Delta D_n \times 10^{-6}$	$n=3$	1.80 ± 0.95	3.68 ± 1.46
	$n=5$	2.12 ± 0.90	2.28 ± 0.79
	$n=7$	2.17 ± 0.68	1.73 ± 0.49

Table 1. Normalized frequency and dissipation shifts for PLL-*g*-PEG and CMD layers at the overtones of $n=3$, 5, 7. The data are presented as averaged values ± standard deviation, calculated from 3 parallel experiments both for PLL-*g*-PEG and CMD.

neglected and Δf, ΔD data only for the overtones of $n>1$ were presented. The data were read at the end point of the corresponding curves in graph **A** and **B** of Fig. 2. The measured $\Delta f_n/n$ values followed only a small dependence on the overtone number, usually suggesting that the Sauerbrey equation could be rather adequate for calculating the deposited mass of PLL-*g*-PEG and CMD layers and therefore these layers were supposed to be rigid. In contrast to this observation, the values of ΔD_n ($>2 \times 10^{-6}$) indicated significant viscoelastic behavior that was particularly expressed in case of CMD. For PLL-*g*-PEG, ΔD_n values ($\approx 2 \times 10^{-6}$) were around the proposed boundary[39,40].

In situ QCM-I measurements enabled to investigate not only the properties of the remained layer at the end of the experiment, but also the progress of layer formation. Comparing the obtained $\Delta f_n/n$ and ΔD_n graphs of CMD and PLL-*g*-PEG in Fig. 2, the data indicate considerable differences in the behavior of the two layers. While most of the adsorbed PLL-*g*-PEG was irreversibly attached to the surface (graph **A**, small change in $\Delta f_n/n$ as a function of time), a significant amount of CMD could be washed off (**B**). It is also clear from graphs **C** and **D**, that the viscoelastic properties were strongly affected by rinsing the layer, demonstrated indirectly by ΔD in time. The relatively high shift in ΔD of PLL-*g*-PEG against the unwashed state suggests that peeling of a small number of weakly bound chains could lead to a perceivable alteration in the rigidity of the layer. The effect of rinsing was much more notable in case of CMD. Despite the frequency shift caused by the formed CMD layer was more than two-folds compared to PLL-*g*-PEG, about 80% of the frequency shift was retrieved by desorbing during the washing and the dissipation of the remained layer turned to $\Delta D_3 = 4.8 \times 10^{-6}$ from a strongly dissipative state ($\Delta D_3 \approx 60 \times 10^{-6}$ compared to the value of 2.5×10^{-6} for PLL-*g*-PEG). Therefore, it is supposed that the CMD layer consisted of mostly loosely bound chains during the deposition phase, providing a soft coverage. Afterwards, these chains were easily desorbed, and a thin covalently grafted film could only remain.

Graphs **E** and **F** clearly illustrate and confirm the effect of washing, where one can track the change of ΔD against Δf in the whole experimental timescale. The significant bend in the CMD curve (graph **F**) originates from the peak in Δf and ΔD during the washing section when intense desorption of the loosely attached chains was in progress. The analysis of this observation supported by OWLS data will be demonstrated in the subsequent part of the Discussion (Section 2.3).

Since the relatively high value of ΔD suggested a viscoelastic case, we used our evaluation code to determine the hydrated mass ($M_A^{QCM,V}$, where V in the superscript refers to the Voigt-based model), shear viscosity (η_A) as well as shear elastic modulus (μ_A) of the adlayers. Beside the measured Δf and ΔD data, the Voigt-based viscoelastic model requires the effective density of hydrated adlayer (ρ_A) as an input parameter. In case of heavily hydrated layers, ρ_A can be approximated with the density of water, thus, $\rho_A = 1000\,kg/m^3$ was used both for CMD and PLL-*g*-PEG[23].

The results computed by fitting the measured Δf and ΔD data are presented in Table 2 (data were given for the end point of the experiment, representing the remained stable layer on the surface), and the obtained fits of measured Δf and ΔD data for one PLL-*g*-PEG and one CMD measurement are shown in Fig. 2. Herein, graph **A**, **B**, **C** and **D** represent the fitted curves for the entire experimental timescale together with the corresponding measurements. Note that during the experimental section of polymer deposition, the resulted data must be carefully considered, because the same fixed bulk parameters (viscosity, modulus and density) were used in the model as in the baseline section, however they were actually unknown. This could be especially true in the case of CMD experiments, where the solution with a relatively high concentration (50 mg/ml) was applied.

The resulted time-dependent surface mass densities are shown in graphs **A** and **B** of Fig. 3 which combine the mass data obtained from OWLS and QCM-I measurements. In addition, graph **C** and **D** represent the thickness as well as **E** and **F** the viscosity and modulus data calculated by the fits. At the bottom, the proposed schematic structures of the attached layers are also depicted (**G**, **H**).

Due to the fact that the measurements with the applied QCM-I instrument have not been reported in the scientific literature before, in order to validate our measured and evaluated data, we compared the results with published ones which were obtained from similar QCM-D experiments or from other reliable techniques. Even for the widely studied PLL-*g*-PEG layers, although mass data are well published, viscoelastic parameters are less available. In the work of Perry *et al.*, 75.2 ng/cm^2 was quantified for the dry mass of PLL-*g*-PEG layer[41] on silica surface using the OWLS technique. The thickness of those layers in hydrated state was found to be 5.91 nm, which is in good agreement with our findings. In another study, where a PLL-*g*-PEG polymer with higher molecular weight PEG was used (PLL(20)-*g*[3.5]-PEG(5)), higher dry (198 ng/cm^2) and wet mass (1241 ng/cm^2) could be observed by OWLS and QCM-D[23]. In order to demonstrate the diversity of the literature values, more reference data are compiled in Table 2. The determined viscoelastic parameters (η_A and μ_A) were higher than the literature

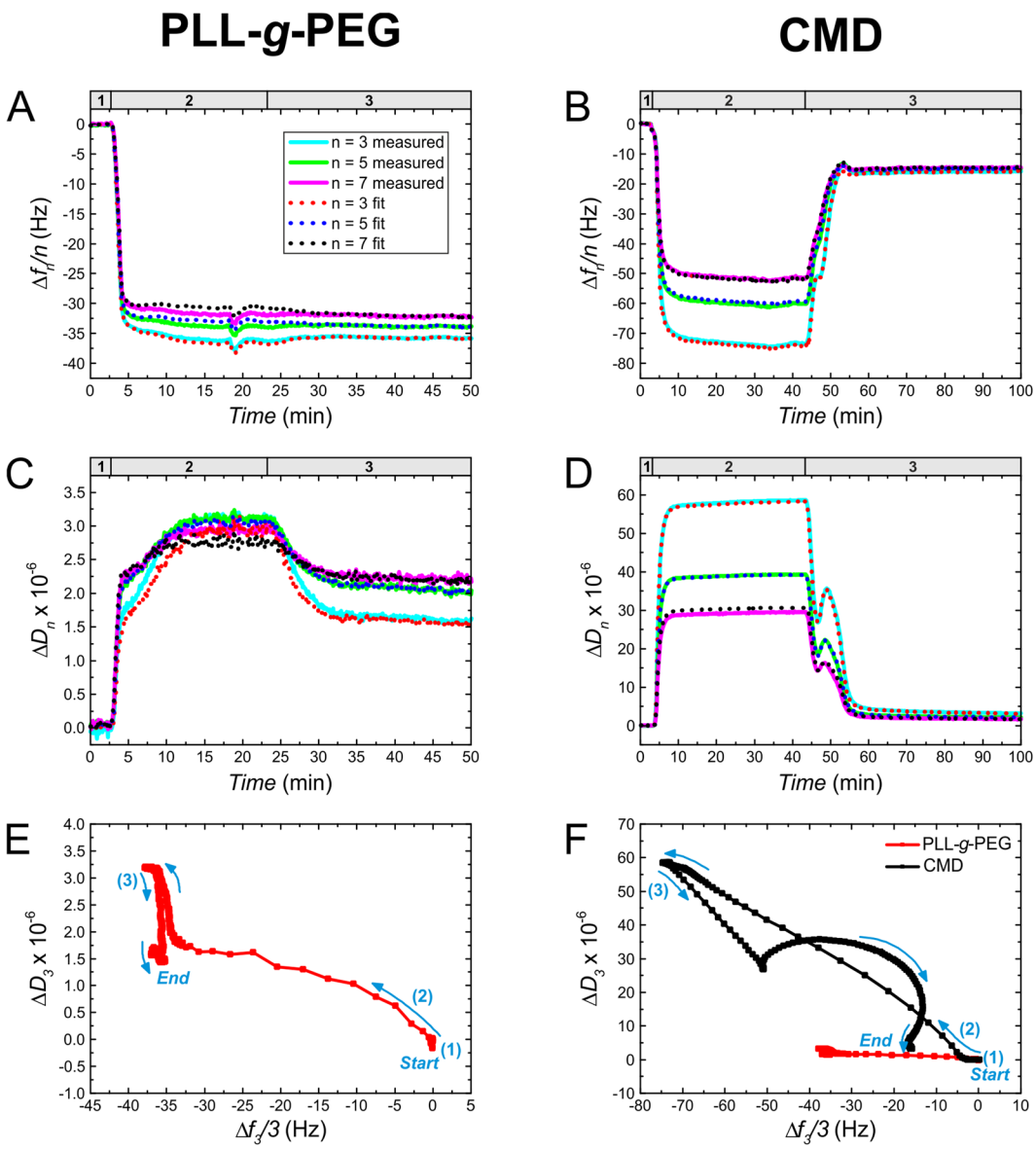

Figure 2. Measured frequency and dissipation shifts as well as corresponding model fits **A**, **B**, **C**, **D**. Normalized frequency (**A**,**B**) and dissipation (**C**,**D**) shift curves measured as a function of time by *in situ* QCM-I on the deposition of PLL-*g*-PEG (**A**,**C**) and CMD layers (**B**,**D**) onto SiO_2-TiO_2 surfaces. The data are plotted for the overtones $n = 3, 5, 7$ (see the legend in graph **A**, which is also related to graph **B**,**C** and **D**). The experiments were performed in three consecutive steps: the polymer-free solution was first driven through the flow-cell to have a stable baseline (1); then the solvent was exchanged to the polymer solution (2), which was flowed until it was replaced by the solvent (3) in order to wash away the loosely adsorbed polymer chains. The model fits of the measured normalized frequency and dissipation shifts for the overtones 3, 5 and 7 are also shown. We quantified the quality of fit for the entire fitted time interval by the mean squared error (MSE) number. In case of the shown fits, MSE = 117 and 22 could be reached for PLL-*g*-PEG and CMD measurements, respectively. (**E**,**F**) Dissipation shift against normalized frequency shift curves for PLL-*g*-PEG (**E**) and CMD (**F**). The arrows show the direction of the experiment in time, while the numbers indicate the specific experimental sections as explained above (1: baseline, 2: deposition, 3: washing). The red curve in plot **E** is enlarged from plot **F**.

data, which can be attributed to the lower water content of the layer. Our results derived from the viscoelastic analysis were in good agreement with published observations, nevertheless they should be considered carefully due to the limitations of the Voinova's model[42].

Since elaborate QCM studies on ultrathin CMD nanolayers are missing in the literature, our data could be only compared with data obtained on similar materials. The reference values for comparison are summarized in Table 2.

Comparison of hydration degrees. While OWLS measures only the deposited mass of the polymer layer without the bound or trapped solvent molecules ("dry mass"), QCM measures the solvated mass of the polymer chains ("wet mass"). Comparing the mass density data derived from OWLS measurements (M_A^{OWLS}) with the

	Measured		Reference[a]	
	PLL-*g*-PEG	CMD	PLL-*g*-PEG or PEG[b]	PLL-*g*-D[c], D[d], CMC[e]
M_A^{OWLS} (ng/cm^2)	274 ± 36	124 ± 23	268 ± 14[43], 198 ± 12[23]	—
$M_A^{QCM,S3}$ (ng/cm^2)	575 ± 66	277 ± 28	—	—
$M_A^{QCM,V}$ (ng/cm^2)	618 ± 36	1102 ± 487	690[43], 1241 ± 63[23]	—
φ_A (%)	56	89	72[43], 83[44], 84[23]	57[43(c)], 60–70[59(c)]
$N_{H_2O/monomer}$	4	71	7[43], 14[23]	14[43(c)], 15–30[59(c)]
ρ_A (kg/m^3)	1000	1000	1000[23]	1000[60(d)]
n_A	1.58 ± 0.04	1.66 ± 0.22	—	—
d_A^{OWLS} (nm)	2.1 ± 0.1	0.9 ± 0.5	—	—
$d_A^{QCM,S3}$ (nm)	5.8 ± 0.7	2.8 ± 0.3	—	—
$d_A^{QCM,V}$ (nm)	6.2 ± 0.4	11.0 ± 4.9	5.9[41], 8.5 ± 0.4[44]	—
η_A (mPa·s)	3.71 ± 1.22	1.43 ± 0.27	1.7[44], 1.4[38(b)]	0.50 ± 0.26[60(d)]
μ_A (MPa)	0.80 ± 0.46	0.029 ± 0.014	0.10[43], 0.125[38(b)]	0.1–0.2[39(e)]

Table 2. Summary and literature review of results obtained from parallel OWLS and QCM-I measurements on PLL-*g*-PEG and CMD layers The data are presented as averaged values ± standard deviation calculated from 3 repeated experiments both for PLL-*g*-PEG and CMD as well as for OWLS and QCM-I measurements. The superscripted indications are devoted to set the following remarks: [a]some referred data were not concretely measured on PLL-*g*-PEG and CMD polymers (see details below); [b]measured on PEG; [c]measured on PLL-*g*-D (D as dextran); [d]measured on dextran; [e]measured on carboxymethyl cellulose (CMC). M_A^{OWLS}: areal mass density measured by OWLS; $M_A^{QCM,S3}$, $M_A^{QCM,V}$: areal mass density measured by QCM-I and evaluated by the Sauerbrey equation as well as by the Voigt-based model, respectively; φ_A: hydration degree; $N_{H_2O/monomer}$: number of bound water molecules per one monomer unit of the polymer chain; ρ_A: density of the hydrated polymer adlayer; n_A, d_A^{OWLS}: refractive index and optical thickness of the adlayer determined by OWLS; $d_A^{QCM,S3}$, $d_A^{QCM,V}$: adlayer thickness evaluated by the Sauerbrey equation as well as by the Voigt-based model, respectively; η_A, μ_A: shear viscosity and shear elastic modulus of the polymer adlayer evaluated by the Voigt-based model. The references are indicated by the numbers in the superscripts.

QCM mass densities calculated by the fit of the Voigt-based model ($M_A^{QCM,V}$) (Table 2) one can conclude that there is a significant difference between the PLL-*g*-PEG and CMD both in the adsorbed amount of polymer chains ("dry mass") and in their hydrated state ("wet mass"). The difference between the dry and wet masses are expressively illustrated in Fig. 3 (graphs **A** and **B**), where the amount of bound water (M_w) in the remained layers is also indicated. Using the two obtained mass data, the hydration degree φ_A with respect to the wet mass can be calculated as follows[20]:

$$\varphi_A = \frac{M_A^{QCM,V} - M_A^{OWLS}}{M_A^{QCM,V}} \times 100 \tag{1}$$

Both for the PLL-*g*-PEG and CMD layers, high water content could be determined, with values of $\varphi_A = 56\%$ and 89%. It is noted that for PLL-*g*-PEG layer a higher hydration of 72–84% can be found in recent reports[23,43,44]. While the dry mass of the polymer chains was lower for the CMD, its hydrated mass significantly exceeded the hydrated mass of PLL-*g*-PEG, suggesting the prominent hydration ability of CMD molecules. The huge difference between the Sauerbrey ($M_A^{QCM,S3}$) and Voigt CMD mass clearly verify the application of the viscoelastic model in the data analysis. The number of bound water molecules per one monomer unit of the polymer chain ($N_{H_2O/monomer}$) was also calculated according to the method of Müller and co-workers[23] (see Table 2).

Kinetic analysis of CMD deposition – conformational changes of polymer chains in terms of hydration and viscoelasticity. To reveal time-dependent changes in the formation of heavily hydrated CMD nanolayers, we developed a novel OWLS-QCM data analyzing methodology based on the quasi-isotropic analysis of OWLS data combined with derivative quantities (hydration degree, viscosity) gained from parallel QCM-I measurements. The conventional quasi-isotropic analysis of optogeometric results calculated from OWLS data using the 4-layer homogenous isotropic mode equations was introduced by Horvath and Ramsden[45], however it has never been applied in combination with QCM data. It was shown that the sign of the deviation between the calculated refractive index (n_A) and expected (realistic) refractive index of adlayer suggests a positive or negative birefringence that can be also expressed by the relation of the ordinary ($n_{A,o}$) and extraordinary ($n_{A,e}$) components of n_A. According to these considerations, if the determined n_A underestimates the expected layer refractive index, the chains are supposed to pose dominantly perpendicular to the surface which is a case of positive birefringence ($n_{A,o} < n_{A,e}$). In case of an overestimated n_A, the prevalent chain conformation is implied to be parallel to the surface (negative birefringence, $n_{A,o} > n_{A,e}$).

Graph **A** of Fig. 4 presents both the n_A and φ_A parameters of CMD layer at the experimental timescale. The refractive index of the bulk dextran[29] (plausible approximation for the refractive index of CMD) and the determined φ_A allowed to estimate the time-dependent values of the CMD layer's realistic refractive index ($n_{A,est}$) and

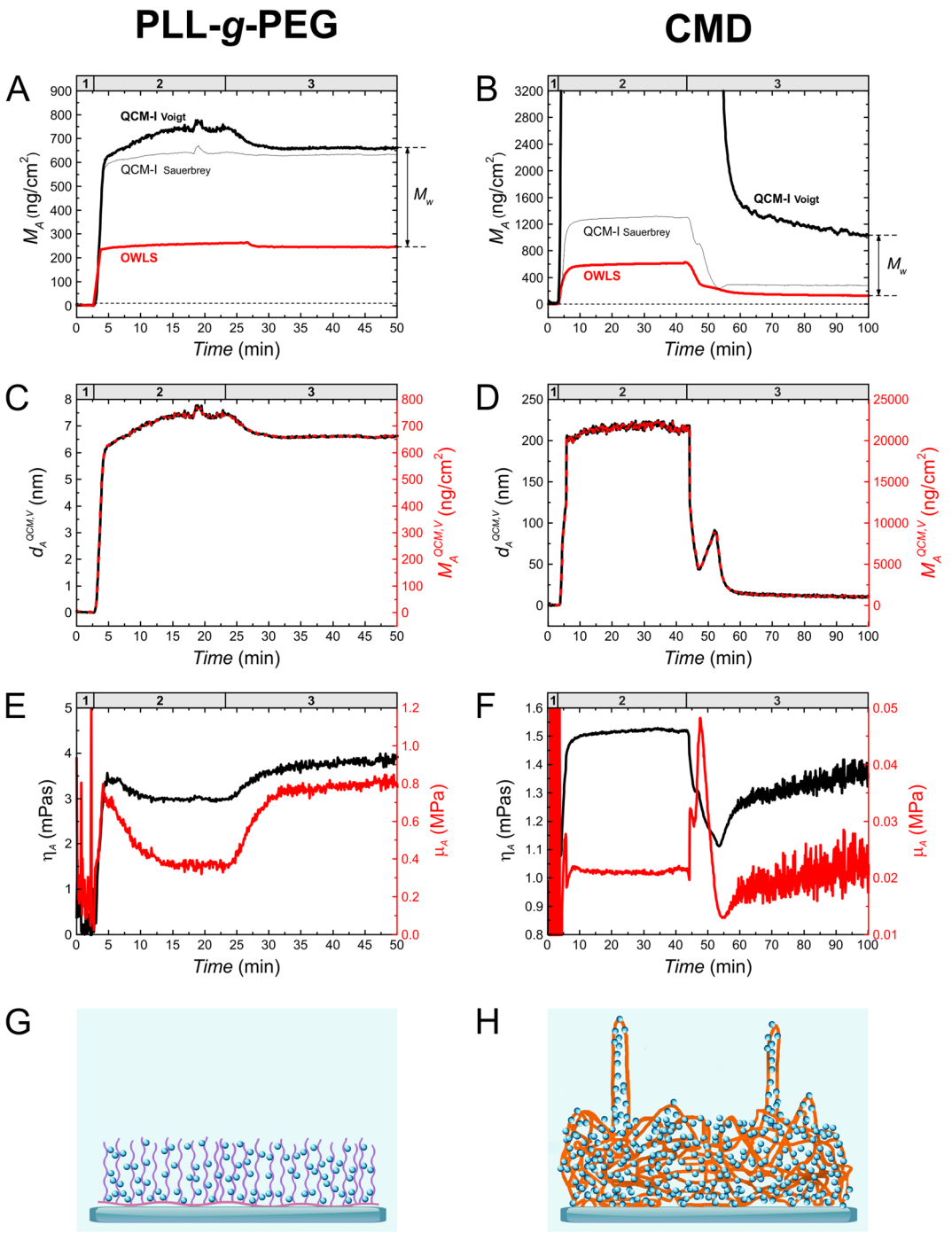

Figure 3. Results from the Voigt-based viscoelastic model and determination of the mass of bound water. (**A**,**B**) Areal mass density sensograms of *in situ* QCM-I (solid black line) and OWLS (solid red line) measurements on PLL-*g*-PEG (**A**) and CMD (**B**) deposition experiments. The numbers in the headers indicate the corresponding experimental sections (detailed in Fig. 2). Two types of QCM-I mass interpretations are plotted. The thicker lines belong to the mass data calculated by the Voigt-based model, while the thinner lines correspond to the 3rd overtone Sauerbrey mass (S3). In case of the CMD plot (**B**), the data of the fitted Voigt mass were smoothed by adjacent-averaging method using a 10-point averaging window. The dashed line underneath is an extension of the baseline. At the deposition section of CMD experiment, the calculated Voigt mass was too high for a proper interpretation, therefore only the masses up to 3200 ng/cm^2 are shown. (**C**,**D**) Full mass (dashed red) as well as thickness plots (solid black curves) are shown in graph **C** and **D**. The thickness and mass curves have the same shape as they are simply proportional by the factor of layer density (Eq. (5), Section 4.4). The layer density was fixed at 1000 kg/m^3. (**E**,**F**) Additional model calculation results as a function of time: shear viscosity (black) and shear elastic modulus (red) of PLL-*g*-PEG and CMD adlayers. (**G**,**H**) The drawings are demonstrating the proposed structure of the formed polymer layers, where both the polymer chains and bound water molecules are indicated.

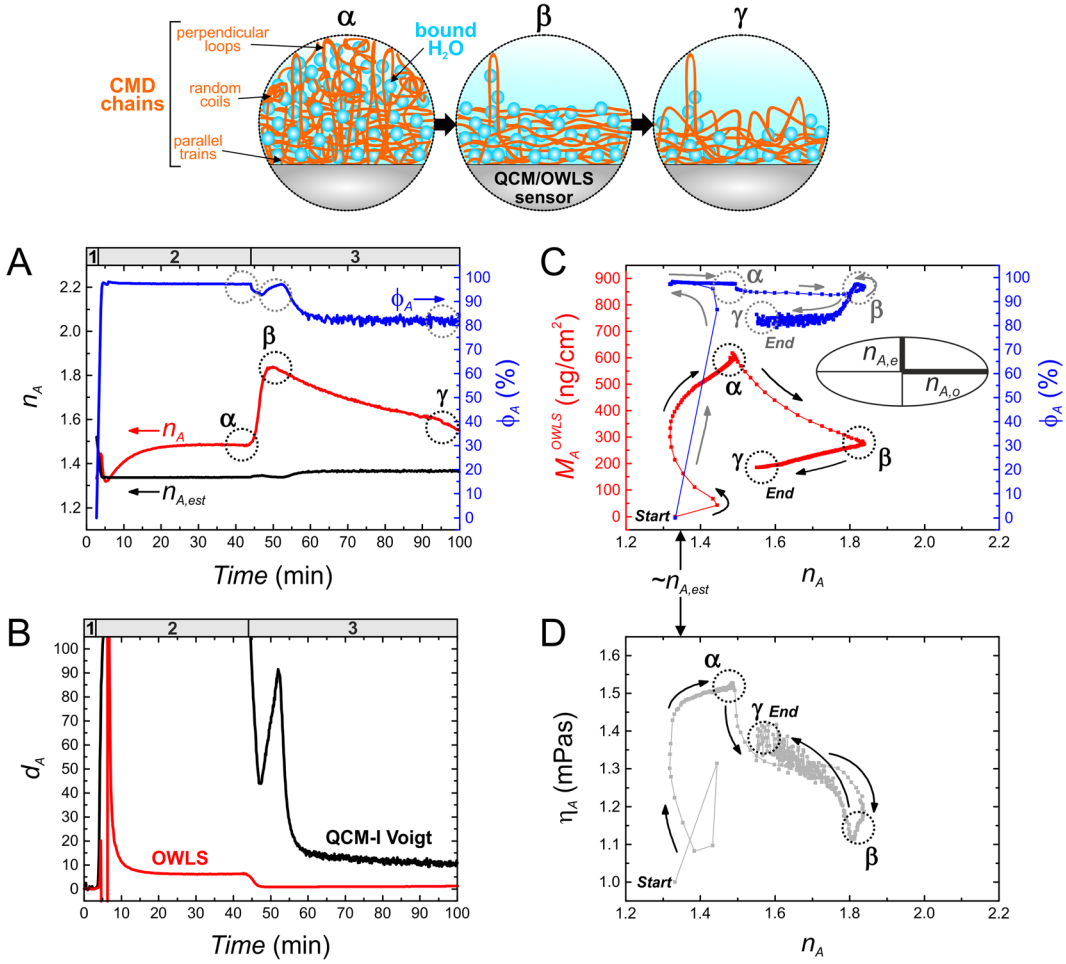

Figure 4. Revealed conformational changes in CMD layers in terms of hydration and viscoelastic properties, based on our developed data analysis methodology and the resulted composite graphs. The illustrations on the top demonstrate the assumed conformational changes in the formed CMD layer, relating to certain experimental phases (times) which are indicated in the corresponding graphs by α, β and γ, respectively. The numbers in the headers indicate the experimental sections which are detailed in Fig. 2. Graph **A** and **B** represent the adlayer refractive index (n_A) and hydration (φ_A) as well as mechanical and optical thickness data (d_A^{OWLS} and $d_A^{QCM,V}$) obtained at the whole experimental timescale. Graph **B** shows the thicknesses originating from both the OWLS and QCM-I measurements, using the same hydrated thickness data of graph **D** in Fig. 3. The values of n_A and d_A were calculated from OWLS measurements using the isotropic homogenous 4-layer mode equations. The estimated (realistic) refractive index of the CMD layer ($n_{A,est}$) was also calculated, based on the known refractive index of bulk dextran and determined hydration degree. These $n_{A,est}$ values (1.33–1.36) provided a practical boundary for the isotropic-anisotropic transition (shown in graph **A**,**C** and **D**). Graph **C** was compiled from n_A and φ_A data of graph **A**, providing useful physical parameters over the measured dry CMD masses (M_A^{OWLS}). In the inset of graph **C**, the refractive index ellipsoid demonstrates the observed negative birefringence in the adlayer ($n_{A,o} > n_{A,e}$). Graph **D** combines the magnitude of anisotropy (n_A) with layer viscosity (η_A), where the latter quantity was independently determined from QCM-I.

to present its time dependence. It was obvious that the applied 4-layer mode equation model provided unrealistic n_A for the whole experiment. Moreover, since the magnitude of this overestimation correlates with the extent of anisotropy[45], the time-dependent changes in the value of n_A allowed to deduce structural changes of the CMD layer. The overestimation of n_A is also expressed in the underestimated values of optical thickness (d_A^{OWLS}) originated from OWLS data as well. In Fig. 4, graph **B** demonstrates the differences to the realistic hydrated thickness obtained from QCM-I measurements.

For the better understanding of conformational alterations, graph **C** and **D** show the curves of the dry CMD mass (M_A^{OWLS}) combined with φ_A as a function of n_A as well as η_A as a function of n_A, respectively. Owing to this special data interpretation that involves time as an implicit parameter, one can track the effect of polymer deposition as well as the effect of washing on the layer structure. Based on the data, the inset figures α, β and γ illustrate the devised layer structures, relating to certain phases of the layer fabrication timescale. The formation and desorption of CMD layer is presented as follows. Right after the CMD solution inflow, a thick, heavily hydrated ($\varphi_A \approx 97\%$) and viscous ($\eta_A \approx 1.52$ mPa·s) layer was formed and stabilized in which the dominant chain

conformation was parallel to the surface (α). The increased magnitude of anisotropy ($n_A = 1.49$ vs. $n_{A,est} = 1.34$) suggests only few perpendicular loops and attached random coils in the layer. However, in the forthcoming washing phase, a huge and fast alteration occurred in the layer structure ($n_A = 1.49 \rightarrow 1.84$) that was induced by the removal of loosely bound chains mostly with perpendicular and random coil conformations. As a result, the remaining layer (at ca. 50 min, indicated by β) consisted of prevalently lain down chains (so-called train conformation) with only very few extending loops.

Nevertheless, an unexpected bend appeared around phase β in the curve of φ_A (see graph **C**, transiently increasing φ_A values). In addition, β was followed by a continuous decrease in n_A and increase in η_A (**D**) presenting an opposite direction to the preceding tendency. The bend corresponds to the indicated peak around β in the time-dependent φ_A curve of graph **A** and it could be originated from the peak appeared in the ΔD_n and $\Delta f_n/n$ curves as well as from the bend in the $\Delta D_3 - \Delta f_3/3$ curve, respectively (Fig. 2B,D,F). Whilst the phenomenon around β could not be perceived by the raw effective refractive index and calculated OWLS mass data, it was clearly revealed by the alteration of n_A. Based on the above considerations, we strongly argue that after the rapid displacement of weakly bound CMD molecules, a conformational rearrangement started in the layer structure, accompanying with a moderate loss of mass and involving the buckling of lain down chains to extending loops (descending n_A). The rearrangement was accompanied with a transient rehydration of the layer (see the small bend in the φ_A curve, graph **C**), followed by a recommencing dehydration that should have been governed by the slight detachment of CMD chains (moderate change in M_A^{OWLS} after β). The presence of chains with higher extension and less hydration is also backed up by the observed rise in layer viscosity (graph **D**).

The fact that the massive decreasing tendency of n_A could be still observed when the surface amount of both the CMD chains and trapped water was stabilized (only small level of mass loss), strongly confirms the conformational rearrangement hypothesis. It is also concluded that despite the emergence of perpendicularly oriented loops, the lain down chains were still dominating in the remained CMD layer structure (γ), as demonstrated by the relatively high n_A values ($1.55 > n_{A,est} = 1.36$, significant negative birefringence).

As it is supported by all the analyzed data (n_A, d_A, M_A^{OWLS}, φ_A, η_A) and due to the fact that separate effects of the conformational rearrangement could be independently detected by OWLS and QCM-I measurements, the presented layer formation mechanism is based on plausible considerations. It is worth highlighting that without the quasi-isotropic analysis, the conformational rearrangement could not have been observed by OWLS (the raw QCM-I data were yet sensitive). Our present results coincide well with our previous findings on the conformational alterations in ultrathin CMD layers[37]. Here we also note that the background of the observed phenomena should be further analyzed due to the complexity (hydrated state, covalent attachment) and nano-scaled dimensions of the examined layers.

Conclusion

In this study, a newly developed QCM-I instrument based on the impedance measurement read-out method has been presented. The QCM-I chips covered by a film of SiO_2-TiO_2 waveguide material provided the ability to have the identical surface chemistry for performing complementary experiments along with the OWLS technique. Electrostatically adsorbed PLL-*g*-PEG and covalently grafted CMD interface layers were deposited and monitored *in situ* by the two biosensor techniques. The well-documented PLL-*g*-PEG was used as a reference system to demonstrate the new QCM-I measurement technique and the developed evaluation methodologies. The results on PLL-*g*-PEG coincide well with the reference data from the literature based on QCM-D measurements, validating the instrument and our QCM-I data evaluation code. Our results on the viscosity, modulus, hydration degree and wet thickness of ultrathin CMD layers have not been published so far to the best of our knowledge. The measurements revealed significant difference between the two polymer nanolayers: the deposited dry mass showed less amount of CMD grafted to the surface than in case of the electrostatically deposited PLL-*g*-PEG. However, the water content of the CMD and PLL-*g*-PEG layer with respect to the solvated mass (hydration degree) was determined to be 89% and 59% revealing a significantly higher hydration capability of the CMD layer. Our evaluation code could be successfully used for viscoelastic analysis: the shear viscosity and shear elastic modulus of the polymer adlayers were determined. The measured data were thoroughly compared with literature values, which can help further studies in layer optimization for biosensing. We developed a novel OWLS-QCM data analysis methodology in order to enlighten the time-dependent structure of CMD nanolayers in terms of hydration and viscoelastic behavior. As a basis, we extended the quasi-anisotropic analysis methodology with the support of QCM-I data. Analyzing the layer formation mechanism, we found that the washing phase induced significant conformational rearrangement in the layer structure resulting in dominantly lain down chains complemented with a moderate number of loop type conformations. The presented results were established by the combined evaluation of anisotropic characteristic, dry mass, hydration degree and layer viscosity.

We successfully demonstrated the ability of our developed analysis protocol that is a useful approach for future investigations of hydrated ultrathin layers based on parallel *in situ* OWLS-QCM measurements.

Methods

Chemicals. The synthetic copolymers, poly(L-lysine)-*graft*-poly(ethylene glycol) (PLL-*g*-PEG, with the architecture of PLL(20)-*g*[3.5]-PEG(2), where the molecular weight of the PLL backbone and the PEG chains were 20 kDa and 2 kDa, respectively, and the grafting density [(lysine-mers)/(PEG side chains)] was 3.5) were obtained in its powder form from SuSoS AG (Dübendorf, Switzerland). 4-(2-hydroxyethyl)-1-piperazineethanesulfonic acid (HEPES) was purchased from Sigma-Aldrich. Dextran T-500 (with 500 kDa molecular weight) was obtained from Pharmacosmos A/S (Holbaek, Denmark). 3-aminopropyltriethoxysilane (hereafter aminosilane), Ethyl-3-(3-dimethylaminopropyl)-carbodiimide hydrochloride (EDC) and N-hydroxysuccinimide (NHS) were obtained from Sigma-Aldrich, monochloroacetic acid was purchased from Thermo Fisher. Water used in the experiments was ultrapure grade Milli-Q water with resistivity of 18 MΩ·cm. All chemicals and reagents were of analytical grade.

Sample preparation. *Sensor chip cleaning.* OWLS chips were cleaned by chromic acid followed by intensive washing with ultrapure water and drying under N_2 stream. QCM-I chips were first washed by ultrapure water and 10 min exposure to UV ozone cleaner (MicroVacuum Ltd., Budapest, Hungary) was subsequently used.

Fabrication of CMD layers. The synthesis of CMD from 500 kDa molecular weight native dextran derived from a published procedure of Huynh *et al.*[46] and it was detailed in our previous work[37]. The sample preparation for CMD grafting and the grafting process itself was also described in our publication[37], however, some modifications were implemented. Cleaned chips surfaces were silylated by 3-aminopropyltriethoxysilane in a heated vacuum chamber (Glass oven B-585, BÜCHI Labortechnik AG, Flawil, Switzerland). 200 µl of the aminosilane was placed into a glass vial that was mounted behind the sample rack in the vacuum chamber. Followed by a 10 min incubation at 80 °C under vacuum (≤5 Hg mm), the samples were held without heating for 20 min, and then they were baked at 120 °C for 2 hours in vacuum. The produced aminated surfaces were kept in vacuum desiccator until used.

The CMD used in this work was characterized by a degree of substitution (DS) of 0.6. The CMD solutions were prepared by dissolving lyophilized CMD in water. The pH of the CMD solution was subsequently adjusted by NaOH to pH 7.0–7.2 and the solution was syringe-filtered on 0.2 µm pore size membrane. NHS and EDC were added to the CMD solution and this so-called grafting solution (CMD-EDC-NHS solution) was used after 15 min of incubation.

The grafting procedure of CMD was performed in particular flow-cells of the related QCM-I and OWLS setups, while the surface deposition was monitored *in situ*. The flow rate was maintained at 1 µl/s by peristaltic pump (Ismatec Reglo, Cole-Parmer GmbH, Wertheim, Germany) throughout the experiment. The experiment started with water flow. After reaching a stable baseline, the water was replaced by the CMD-EDC-NHS solution, which was flowed through the cell for 40 min. Afterwards, water was used again for washing the surface until a constant signal could be recorded.

Fabrication of PLL-g-PEG layers. PLL-*g*-PEG solutions with concentration of 1 mg/ml were prepared in HEPES buffer (with HEPES concentration of 10 mM). The pH of the HEPES was adjusted by NaOH solution to 7.4 before the preparation of the PLL-*g*-PEG solution. The sensor chip surfaces were not chemically modified, they were used in the experiments after the cleaning process. Followed by reaching a stable baseline with HEPES that was also driven by a peristaltic pump (flow rate was 1 µl/s throughout the experiment), the PLL-*g*-PEG solutions were flowed over the sensor chip for 20 min. The washing section was performed with HEPES flow until a constant signal was reached.

Measurement techniques. *Optical waveguide lightmode spectroscopy (OWLS).* Optical waveguide lightmode spectroscopy measurements were performed by an ASI BIOS-1 and OWLS 210 instruments (MicroVacuum Ltd., Budapest, Hungary). The optical sensor chips consist of a SiO_2-TiO_2 waveguide layer on top of an AF45 glass substrate. The 2400 µV and OW2400 type sensor chips were obtained from MicroVacuum Ltd. The linearly polarized 632.8 nm wavelength He-Ne laser beam was coupled into the waveguide layer by the grating imprinted on the sensor chip. *In situ* measurements were conducted by assembling the chip with a flow-cell, which was set in the goniometer of the instrument. The liquid was flowed over the waveguide surface at a 1 µl/s flow rate by employing a peristaltic pump (Ismatec, Reglo). The coupling angle was scanned with 14 s time resolution.

The refractive indices of the solutions (n_c) were measured separately by a precision refractometer at the wavelength of 632.8 nm (J157 Automatic refractometer, Rudolph Research Analytical). The recorded OWLS data were evaluated by the 4 layer mode equations[47] and the surface mass density was calculated using the de Feijter's formula[48]. (Data for the calculations: $dn/dc_{CMD} = 0.15\ cm^3/g$, $dn/dc_{PLL\text{-}g\text{-}PEG} = 0.139\ cm^3/g$, $n_{HEPES} = 1.332$, $n_{water} = 1.3317$; where dn/dc is the refractive index increment of the solution of the applied polymer, n is the refractive index of the solution indicated by the given subscript. All refractive index data belong to the wavelength of 632.8 nm).

Quartz crystal microbalance with impedance measurement (QCM-I). The applied QCM setup was a QCM-I instrument from MicroVacuum Ltd. (Budapest, Hungary)[49]. The resonance sensitivity of the instrument in liquid is 2×10^{-1} Hz, the dissipation sensitivity is 1×10^{-7} and the mass sensitivity is $\leq 1\ ng/cm^2$, respectively. The flow-cell volume is ~40 µl. The QCM-I sensor chips used in this work were AT-cut crystals with a diameter of 14 mm and a fundamental resonance frequency of 5 MHz. The fabrication of the SiO_2-TiO_2 layer on top of the gold is based on the sol-gel method used for the OWLS sensors chip fabrication, and it is prepared in the same composition. The *in situ* experiments were performed at 1 µl/s flow rate maintained by a peristaltic pump. The resonance frequency and dissipation shifts were recorded with the time resolution of 6.2 s for each selected overtone (the overtone numbers were $n = 1, 3, 5, 7$ for the frequencies of 5, 15, 25, 35 MHz, respectively). For the development of the evaluation code, MATLAB® (MathWorks, Inc., Natick, USA) was used as programming environment. The employed QCM-I setup and the methodology of data analysis are illustrated in Fig. 5.

Viscoelastic analysis of QCM data – implementation in MATLAB. In the widely used QCM-D technique, the amplitude of the recorded oscillation decay (measured electric current as a function of time) is fitted using the parameters of decay time (τ) and frequency (f) which provide the dimensionless dissipation (D) as follows:

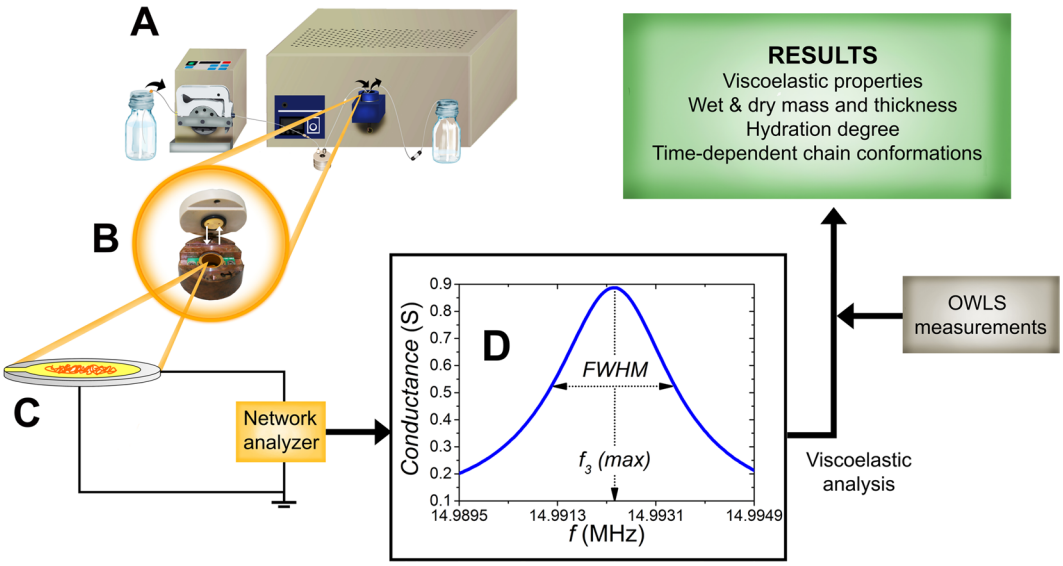

Figure 5. QCM-I measurement setup (**A**) and data evaluation methodology. PLL-*g*-PEG or CMD solutions were flowed into the flow-cell (enlarged in image **B**), where the solution could be facing to the surface of the sensor chip (**C**). Applying a network analyzer, QCM-I measures the frequency spectrum of the conductance (impedance). An obtained resonance peak can be seen around the third overtone resonance frequency (f_3) in graph **D**. Two parameters are quantified by fitting the data points: full width at half maximum (FWHM), proportional to the dissipation as well as resonance frequency at the peak maximum ($f_3(\max) = f_3$). The impedance analysis is performed for each overtone at each measurement time and the *in situ* data provide the basis of the calculations on surface mass density of the interface layer as well as its viscoelastic properties. Complementing the QCM-I results with mass data obtained from OWLS measurements was the basis of determining the hydration degree of the examined polymer layers.

$$D = \frac{1}{Q} = \frac{1}{\pi f \tau} = \frac{E_{dissipated}}{2\pi E_{stored}} \tag{2}$$

where Q denotes the quality factor, $E_{\text{dissipated}}$ is the energy dissipated during one oscillatory cycle and E_{stored} is the energy stored in the oscillating system. The energy dissipation of the quartz crystal can be obtained as the energy dissipation factor D that is the inverse of the frequency quality factor Q. The viscoelastic properties of the polymer layers on a QCM crystal can be described by the D value[50,51]. The f and D values measured for multiple overtones allow to deduce the mass and viscoelastic characteristic of the crystal based on continuum mechanical models, most commonly on the Voigt-Kelvin model developed by Voinova and co-workers[52].

In contrast to the QCM-D, QCM-I applies the impedance analysis as read-out technique. In this case, impedance spectra are recorded for fundamental and overtone frequencies and these spectra are fitted by resonance curves with FWHM (full width at half maximum) and f parameters. As it has been shown by the model of electric circuit approach developed by Johannsmann[53], the formula $\Delta\text{FWHM}/\Delta f$ can be associated with the viscoelastic properties of the crystal and its overlayers, thus viscoelastic analysis by the impedance measurement technique is also available. Dissipation can be expressed by the FWHM parameter derived from the impedance analysis:

$$D = \frac{1}{Q} = \frac{FWHM}{f} \tag{3}$$

It has been also shown, that the impedance spectrum is retrievable from the oscillation decay by Fourier-transformation[24]. As a result, the two D values obtained from the different read-out methods (i.e. QCM-D and QCM-I) can be treated to be equal. Zhang *et al.* pointed out that data recorded by a QCM-D instrument can be accurately evaluated in terms of viscoelastic properties by the equivalent circuit approach[54], which also works vice versa for the evaluation of data obtained by a QCM-I setup using the Voigt-based model.

The Sauerbrey equation gives a linear relationship between the normalized form of the frequency shift ($\Delta f_n/n$) and added mass per unit area ($\Delta M_A^{\text{QCM,S}}$)[55]:

$$\Delta M_A^{QCM,S} = -C\frac{\Delta f_n}{n} \tag{4}$$

where C is the mass sensitivity constant that is dependent only on the physical properties of the quartz crystal, n is the overtone number and Δf_n refers to the frequency shift at a given time t ($f(t=0) - f(t)$) at a given n overtone. Instead of ΔM_A, hereafter the calculated mass will be indicated by M_A.

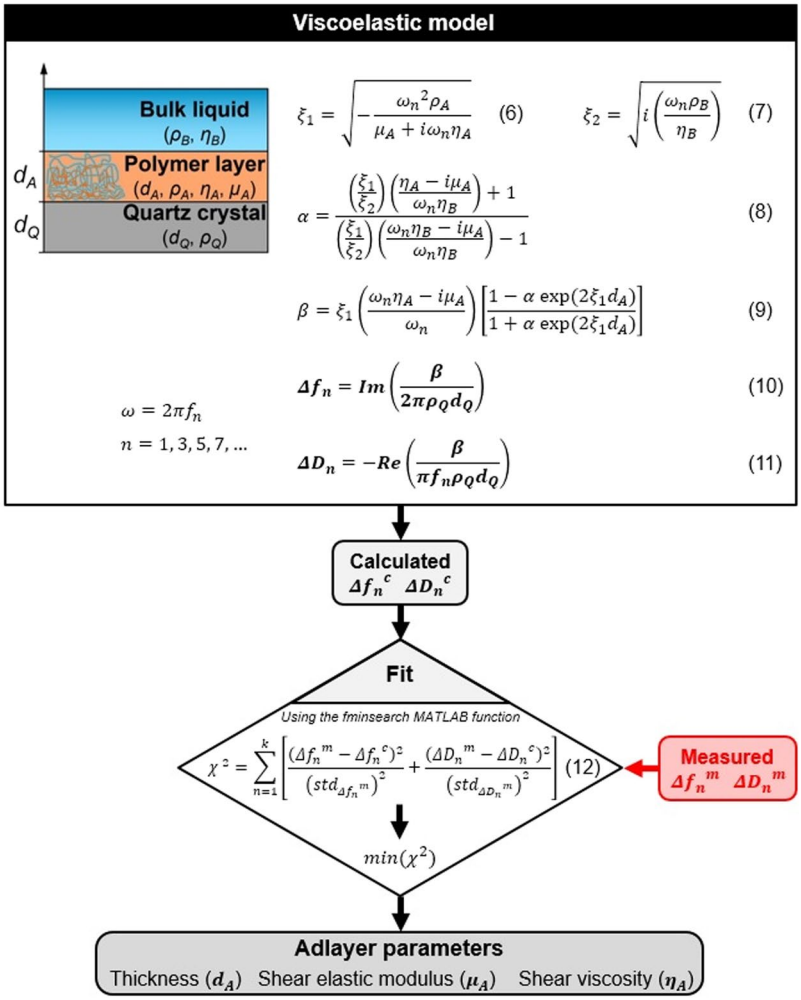

Figure 6. Schematic representation of the QCM data analysis code implemented in MATLAB. In the inset figure on the left upper side, one can see the structure of the applied model where the QCM chip was covered by one viscoelastic film consisted of the deposited polymer chains. The used equations of the Voigt-based model can be seen in the scheme[52], where ρ_Q and h_Q are the density and thickness of the crystal respectively, ρ_B and η_B are the density and viscosity of the bulk liquid as well as ω_n is the angular frequency of the oscillation at a given n overtone. The hydrated thickness, density, shear viscosity and shear elastic modulus of the examined adlayer are represented by d_A, ρ_A, η_A and μ_A, respectively. In the calculation of the error function χ^2 the Δf_n^m, Δf_n^c as well as ΔD_n^m, ΔD_n^c are the measured and computed frequency and dissipations, respectively, the std values correspond to the standard deviations of the measured frequencies and dissipation at the baseline and k denotes the highest overtone number.

Several criteria must be fulfilled for being able to precisely apply the Sauerbrey equation. These criteria demand the examined films to be thin, rigid and evenly distributed on the sensor surface[56]. Especially polymer-based and biological samples tend to be soft and have viscoelastic behavior, causing that their layers cannot entirely follow the motion of the crystal during the QCM measurement. For such layers, the application of the Sauerbrey equation becomes limited, highlighting the need to consider their viscoelastic behavior. A model based on a Voigt viscoelastic element is used to calculate the accurate mass, and additionally, it provides the viscoelastic parameters of the examined layer. This model represents the added viscoelastic layer on the elastic QCM crystal as a viscoelastic element consisted of a spring (elastic part) and dashpot (viscous part). Measuring both the frequency (Δf) and dissipation shifts ($\Delta D = D(t=0) - D(t)$) as a function of time enables the quantitative *in situ* analysis of the thickness (d_A), shear viscosity (η_A) and shear elastic modulus (μ_A) of the interface adlayer.

Areal mass density of the adlayer (M_A^{QCM}) can be calculated from the resulted uniform thickness d_A in case of a given effective mass density (ρ_A):

$$M_A^{QCM} = d_A \rho_A \tag{5}$$

To calculate the viscoelastic parameters of the film, we developed an evaluation code and a graphical user interface (GUI) in MATLAB environment based on the viscoelastic model elaborated by Voinova and co-workers[52], as it is also used in the commercial QTools program which is distributed for QCM-D instruments.

An important aid was provided for the model implementation by a study of McNamara *et al.*, which published a well-documented MATLAB code for predicting the viscoelastic parameters of films by the Voigt-based model with the purpose of giving support to experimental design in QCM measurements[57]. Our program takes the measured Δf and ΔD values at the selected overtones for each measurement time and fits the parameters of the adlayer (d_A, η_A, μ_A) using the MATLAB built-in *fminsearch* function to find the minimum of the sum of squares of the scaled errors[58] (χ^2) between the experimental and model Δf and ΔD values by the simplex method. For the used model equations and schematic representation of the program see Fig. 6. The density and viscosity of the bulk liquid (buffer or pure water) were assumed to be 1000 kg/m^3 and 1.0 mPa·s, respectively. The ρ_A density of the adlayer was also beforehand estimated and fixed at 1000 kg/m^3.

References

1. *Label-free Biosensors. Label-free Biosensors* (Cambridge University Press, 2009).
2. Fang, Y. Label-Free Biosensors for Cell Biology. *Int. J. Electrochem.* **2011**, 1–16 (2011).
3. Orgovan, N. *et al.* Bulk and surface sensitivity of a resonant waveguide grating imager. *Appl. Phys. Lett.* **104**, 83506 (2014).
4. Horvath, R., Pedersen, H. C. & Cuisinier, F. J. G. Guided wave sensing of polyelectrolyte multilayers. *Appl. Phys. Lett.* **88**, 111102 (2006).
5. Picart, C. *et al.* Determination of structural parameters characterizing thin films by optical methods: A comparison between scanning angle reflectometry and optical waveguide lightmode spectroscopy. *J. Chem. Phys.* **115**, 1086–1094 (2001).
6. Farkas, E. *et al.* Self-assembled, nanostructured coatings for water oxidation by alternating deposition of Cu-branched peptide electrocatalysts and polyelectrolytes. *Chem. Sci.* **7**, 5249–5259 (2016).
7. Vörös, J. *et al.* Optical grating coupler biosensors. *Biomaterials* **23**, 3699–3710 (2002).
8. Orgovan, N. *et al. In-situ* and label-free optical monitoring of the adhesion and spreading of primary monocytes isolated from human blood: Dependence on serum concentration levels. *Biosens. Bioelectron.* **54**, 339–344 (2014).
9. Orgovan, N. *et al.* Dependence of cancer cell adhesion kinetics on integrin ligand surface density measured by a high-throughput label-free resonant waveguide grating biosensor. *Sci. Rep.* **4**, 4034 (2014).
10. Kozma, P., Hámori, A., Kurunczi, S., Cottier, K. & Horvath, R. Grating coupled optical waveguide interferometer for label-free biosensing. *Sensors Actuators B Chem.* **155**, 446–450 (2011).
11. Vörös, J. The Density and Refractive Index of Adsorbing Protein Layers. *Biophys. J.* **87**, 553–561 (2004).
12. Höök, F. *et al.* A comparative study of protein adsorption on titanium oxide surfaces using *in situ* ellipsometry, optical waveguide lightmode spectroscopy, and quartz crystal microbalance/dissipation. *Colloids Surfaces B Biointerfaces* **24**, 155–170 (2002).
13. Ismail, I. M., Gray, N. D. & Owen, J. R. A QCM analysis of water absorption in lithium polymer electrolytes. *J. Chem. Soc. Faraday Trans.* **92**, 4115 (1996).
14. Marx, K. A. Quartz Crystal Microbalance: A Useful Tool for Studying Thin Polymer Films and Complex Biomolecular Systems at the Solution−Surface Interface. *Biomacromolecules* **4**, 1099–1120 (2003).
15. Laos, K., Parker, R., Moffat, J., Wellner, N. & Ring, S. G. The adsorption of globular proteins, bovine serum albumin and β-lactoglobulin, on poly-l-lysine–furcellaran multilayers. *Carbohydr. Polym.* **65**, 235–242 (2006).
16. Kittle, J. D. *et al.* Equilibrium Water Contents of Cellulose Films Determined via Solvent Exchange and Quartz Crystal Microbalance with Dissipation Monitoring. *Biomacromolecules* **12**, 2881–2887 (2011).
17. Höök, F. *et al.* Variations in Coupled Water, Viscoelastic Properties, and Film Thickness of a Mefp-1 Protein Film during Adsorption and Cross-Linking: A Quartz Crystal Microbalance with Dissipation Monitoring, Ellipsometry, and Surface Plasmon Resonance Study. *Anal. Chem.* **73**, 5796–5804 (2001).
18. Köβlinger, C. *et al.* Comparison of the QCM and the SPR method for surface studies and immunological applications. *Sensors Actuators B Chem.* **24**, 107–112 (1995).
19. Malmström, J., Agheli, H., Kingshott, P. & Sutherland, D. S. Viscoelastic modeling of highly hydrated laminin layers at homogeneous and nanostructured surfaces: Quantification of protein layer properties using QCM-D and SPR. *Langmuir* **23**, 9760–9768 (2007).
20. Halthur, T. J. & Elofsson, U. M. Multilayers of Charged Polypeptides As Studied by *in Situ* Ellipsometry and Quartz Crystal Microbalance with Dissipation. *Langmuir* **20**, 1739–1745 (2004).
21. Bittrich, E. *et al.* Protein adsorption on and swelling of polyelectrolyte brushes: A simultaneous ellipsometry-quartz crystal microbalance study. *Biointerphases* **5**, 159 (2010).
22. Rodenhausen, K. B. *et al.* Micelle-assisted bilayer formation of cetyltrimethylammonium bromide thin films studied with combinatorial spectroscopic ellipsometry and quartz crystal microbalance techniques. *Thin Solid Films* **519**, 2821–2824 (2011).
23. Müller, M. T., Yan, X., Lee, S., Perry, S. S. & Spencer, N. D. Lubrication Properties of a Brushlike Copolymer as a Function of the Amount of Solvent Absorbed within the Brush. *Macromolecules* **38**, 5706–5713 (2005).
24. Johannsmann, D. *The Quartz Crystal Microbalance in Soft Matter Research*, https://doi.org/10.1007/978-3-319-07836-6 (Springer International Publishing, 2015).
25. Rodahl, M., Höök, F., Krozer, A., Brzezinski, P. & Kasemo, B. Quartz crystal microbalance setup for frequency and Q - factor measurements in gaseous and liquid environments Quartz crystal microbalance setup for frequency and G!? -factor rneasurements in gaseous and liquid environments. *Rev. Sci. Instrum.* **66**, 3924–3930 (1995).
26. Löfås, S. & Johnsson, B. A novel hydrogel matrix on gold surfaces in surface plasmon resonance sensors for fast and efficient covalent immobilization of ligands. *J. Chem. Soc., Chem. Commun.* 1526–1528, https://doi.org/10.1039/C39900001526 (1990).
27. Österberg, E. *et al.* Comparison of polysaccharide and poly(ethylene glycol) coatings for reduction of protein adsorption on polystyrene surfaces. *Colloids Surfaces A Physicochem. Eng. Asp.* **77**, 159–169 (1993).
28. Dubois, J., Gaudreault, C. & Vermette, P. Biofouling of dextran-derivative layers investigated by quartz crystal microbalance. *Colloids Surfaces B Biointerfaces* **71**, 293–299 (2009).
29. Piehler, J., Brecht, A., Hehl, K. & Gauglitz, G. Protein interactions in covalently attached dextran layers. *Colloids Surfaces B Biointerfaces* **13**, 325–336 (1999).
30. Kenausis, G. L. *et al.* Poly(L-lysine)-g-Poly(ethylene glycol) Layers on Metal Oxide Surfaces: Attachment Mechanism and Effects of Polymer Architecture on Resistance to Protein Adsorption. *J. Phys. Chem. B* **104**, 3298–3309 (2000).
31. Huang, N. *et al.* Poly(l-lysine)-g-poly(ethylene glycol) Layers on Metal Oxide Surfaces: Surface-Analytical Characterization and Resistance to Serum and Fibrinogen Adsorption Poly(L-lysine)-g-poly(ethylene glycol) Layers on Metal Oxide Surfaces: Surface-An. *Langmuir* **17**, 489–498 (2001).
32. Chen, S., Li, L., Zhao, C. & Zheng, J. Surface hydration: Principles and applications toward low-fouling/nonfouling biomaterials. *Polymer (Guildf).* **51**, 5283–5293 (2010).
33. Tanaka, M., Hayashi, T. & Morita, S. The roles of water molecules at the biointerface of medical polymers. *Polym. J.* **45**, 701–710 (2013).
34. McLean, K. M. *et al.* Method of immobilization of carboxymethyl-dextran affects resistance to tissue and cell colonization. *Colloids Surfaces B Biointerfaces* **18**, 221–234 (2000).
35. Monchaux, E. & Vermette, P. Development of Dextran-Derivative Arrays To Identify Physicochemical Properties Involved in Biofouling from Serum. *Langmuir* **23**, 3290–3297 (2007).
36. Akkoyun, A. & Bilitewski, U. Optimisation of glass surfaces for optical immunosensors. *Biosens. Bioelectron.* **17**, 655–664 (2002).

37. Saftics, A. *et al*. Fabrication and characterization of ultrathin dextran layers: Time dependent nanostructure in aqueous environments revealed by OWLS. *Colloids Surfaces B Biointerfaces* **146**, 861–870 (2016).
38. Dutta, A. K. & Belfort, G. Adsorbed gels versus brushes: Viscoelastic differences. *Langmuir* **23**, 3088–3094 (2007).
39. Liu, Z., Choi, H., Gatenholm, P. & Esker, A. A. R. Quartz crystal microbalance with dissipation monitoring and surface plasmon resonance studies of carboxymethyl cellulose adsorption onto regenerated cellulose surfaces. *Langmuir* **27**, 8718–28 (2011).
40. Vogt, B. D., Lin, E. K., Wu, W. I. & White, C. C. Effect of film thickness on the validity of the sauerbrey equation for hydrated polyelectrolyte films. *J. Phys. Chem. B* **108**, 12685–12690 (2004).
41. Perry, S. S. *et al*. Tribological Properties of Poly(l-lysine)-*graft*-poly(ethylene glycol) Films: Influence of Polymer Architecture and Adsorbed Conformation. *ACS Appl. Mater. Interfaces* **1**, 1224–1230 (2009).
42. Reviakine, I., Johannsmann, D. & Richter, R. P. Hearing What You Cannot See and Visualizing What You Hear: Interpreting Quartz Crystal Microbalance Data from Solvated Interfaces. *Anal. Chem.* **83**, 8838–8848 (2011).
43. Nalam, P. C. *et al*. Two-Fluid Model for the Interpretation of Quartz Crystal Microbalance Response: Tuning Properties of Polymer Brushes with Solvent Mixtures. *J. Phys. Chem. C* **117**, 4533–4543 (2013).
44. Heuberger, M., Drobek, T. & Vörös, J. About the Role of Water in Surface-Grafted Poly(ethylene glycol) Layers. *Langmuir* **20**, 9445–9448 (2004).
45. Horvath, R. & Ramsden, J. J. Quasi-isotropic Analysis of Anisotropic Thin Films on Optical Waveguides. *Langmuir* **23**, 9330–9334 (2007).
46. Huynh, R., Chaubet, F. & Jozefonvicz, J. Carboxymethylation of dextran in aqueous alcohol as the first step of the preparation of derivatized dextrans. *Die Angew. Makromol. Chemie* **254**, 61–65 (1998).
47. Tiefenthaler, K. & Lukosz, W. Sensitivity of grating couplers as integrated-optical chemical sensors. *J. Opt. Soc. Am. B* **6**, 209 (1989).
48. De Feijter, J., Benjamins, J. & Veer, F. Ellipsometry as a tool to study the adsorption behavior of syntetic and biopolyers at the air water interface. *Biopolymers* **17**, 1759–1772 (1978).
49. MicroVacuum, L. QCM-myQuartz Crystal Microbalanace With Impedance Measurement. Available at: http://www.owls-sensors.com/qcm-i-quartz-crystal-microbalance-with-impedance-measurement.
50. Rodahl, M., Höök, F. & Kasemo, B. QCM Operation in Liquids: An Explanation of Measured Variations in Frequency and Q Factor with Liquid Conductivity. *Anal. Chem.* **68**, 2219–2227 (1996).
51. Höök, F., Rodahl, M., Kasemo, B. & Brzezinski, P. Structural changes in hemoglobin during adsorption to solid surfaces: Effects of pH, ionic strength, and ligand binding. *Proc. Natl. Acad. Sci.* **95**, 12271–12276 (1998).
52. Voinova, M. V., Rodahl, M., Jonson, M. & Kasemo, B. Viscoelastic Acoustic Response of Layered Polymer Films at Fluid-Solid Interfaces: Continuum Mechanics Approach. *Phys. Scr.* **59**, 391–396 (1999).
53. Johannsmann, D. Viscoelastic, mechanical, and dielectric measurements on complex samples with the quartz crystal microbalance. *Phys. Chem. Chem. Phys.* **10**, 4516–4534 (2008).
54. Zhang, Y. *et al*. Convergence of Dissipation and Impedance Analysis of Quartz Crystal Microbalance Studies Convergence of Dissipation and Impedance Analysis of Quartz Crystal Microbalance Studies. *Anal. Chem.* **81**, 642–648 (2009).
55. Sauerbrey, G. V. von Schwingquarzen zur Wagungdiinner Schichten und zur Mikrowagung. *Zeitschrift fur Phys.* **155**, 206–222 (1959).
56. Doliška, A., Ribitsch, V., Stana Kleinschek, K. & Strnad, S. Viscoelastic properties of fibrinogen adsorbed onto poly(ethylene terephthalate) surfaces by QCM-D. *Carbohydr. Polym.* **93**, 246–255 (2013).
57. McNamara, T. P. & Blanford, C. F. A sensitivity metric and software to guide the analysis of soft films measured by a quartz crystal microbalance. Analyst, https://doi.org/10.1039/C6AN00143B (2016).
58. Stengel, G., Höök, F. & Knoll, W. Viscoelastic modeling of template-directed DNA synthesis. *Anal. Chem.* **77**, 3709–3714 (2005).
59. Perrino, C. Poly(L-lysine)-g-dextran (PLL-g-dex): brush-forming, biomimetic carbohydrate chains that inhibit fouling and promote lubricity. (2009).
60. Kuhner, M. & Sackmann, E. Ultrathin hydrated dextran films grafted on glass: Preparation and characterization of structural, viscous, and elastic properties by quantitative microinterferometry. *Langmuir* **12**, 4866–4876 (1996).

Acknowledgements

This work was funded by the Momentum Program ("Lendület") of the Hungarian Academy of Sciences and by the ERC-HU, VEKOP and KH_17 Programs of NKFIH. Support from the János Bolyai Research Scholarship (SK) of the Hungarian Academy of Sciences as well as the Pro Progressio Foundation and Varga József Foundation (AS) are also gratefully acknowledged. We are also grateful for fruitful discussions with Prof. Janos Vörös. The continuous support of MicroVacuum Ltd. is gratefully acknowledged too.

Author Contributions

A.S. performed all experiments. B.P. and B.T. helped in the experiments. A.S., G.A.P. and R.H. developed the evaluation code to analyze the QCM-I data. A.S. analyzed the data and made the figures and tables with the help of B.P. G.A.P. and R.H. performed preliminary QCM-I experiments to set up the device. The CMD applied in the experiments was synthesized and characterized by B.T. S.K. led the work of CMD fabrication and characterization. A.S., S.K. and R.H. wrote the paper. All authors commented on the manuscript. R.H. supervised the projects giving the framework of the present study.

Additional Information

Competing Interests: The authors declare no competing interests.

Publisher's note: Springer Nature remains neutral with regard to jurisdictional claims in published maps and institutional affiliations.

Open Access This article is licensed under a Creative Commons Attribution 4.0 International License, which permits use, sharing, adaptation, distribution and reproduction in any medium or format, as long as you give appropriate credit to the original author(s) and the source, provide a link to the Creative Commons license, and indicate if changes were made. The images or other third party material in this article are included in the article's Creative Commons license, unless indicated otherwise in a credit line to the material. If material is not included in the article's Creative Commons license and your intended use is not permitted by statutory regulation or exceeds the permitted use, you will need to obtain permission directly from the copyright holder. To view a copy of this license, visit http://creativecommons.org/licenses/by/4.0/.

© The Author(s) 2018